Buckling Behavior of Different Types of Spherical Weave Structures Under Vertical Compression Loads

Guang-Kai Song[1] and Bo-Hua Sun*[1]

[1] *School of Civil Engineering Institute of Mechanics and Technology*
Xian University of Architecture and Technology, Xian 710055, China
* *Corresponding author: B.H.S. email: sunbohua@xauat.edu.cn*

Weaving technology can convert two-dimensional structures such as ribbons into three-dimensional structures by specific connections. However, most of the 3D structures fabricated by conventional weaving methods using straight ribbons have some topological defects. In order to obtain smoother continuous 3D surface structures, Baek et al.[1] proposed a novel weaving method using naturally curved (in-plane) ribbons to fabricated three-dimensional curved structures and using this method to weave new spherical weave structures that are closer to perfect spheres. We believe that this new spherical weave structure with smooth geometric properties must correspond to new mechanical properties. To this end, we investigated the buckling characteristics of different types of spherical weave structures by the combination of test and finite element method. The results of calculations and experiments show that the failure mode of the spherical weave structure under vertical loading can be divided into two stages: a flat contact region forms between the spherical weave structure and the rigid plate and inward dimple of ribbons. The spherical weave structures using naturally curved (in-plane) ribbon weaving have better buckling stability than those woven with straight ribbons. The vertical buckling load of spherical weave structures using naturally curved ribbon increases with the width and thickness of the ribbon. In addition, this paper combines test, theoretical and finite element analysis to propose the buckling load equation and buckling correction factor equation for the new spherical weave structure under vertical compression load.

Keywords: Spherical weave structure, In-plane curvatures,Buckling, Test, Buckling load

I. INTRODUCTION

Weaving is a more mature three-dimensional structure forming technology. People can make two-dimensional ribbons, rods, etc. into three-dimensional structures by weaving technology. However, the traditional weaving technology in the production of three-dimensional structure using straight ribbons, straight rod members as the basic components, so there are some serious topological defects in the three-dimensional woven structure. It has been realized so far that how to form some curved 3D structures with continuous geometry and small topological defects using planar structures such as ribbons or rods has been a huge challenge. To address this problem, Baek et al. [1] proposed a 3D surface forming method based on traditional weaving technology, containing ribbons with in-plane curvatures to weave, and using rivets to fix between ribbons. The three-dimensional woven structure formed by this method has fewer topological defects, smoother and more continuous 3D surface structure, and its Gaussian curvature is closer to a continuum. In addition, Baek et al. [1] produced spherical weave structures by arranging the position and number of pentagonal and hexagonal weave structures in a rational combination, and compared with the spherical weave structure formed by the straight ribbon, we found that topological defects of spherical weaves with curved ribbon is within 1%, and and its geometric configuration is closer to a perfect spherical shell structure.

It is well known that spherical shell structure is widely used in architecture, aerospace and other fields because of its light weight and high strength mechanical properties. Therefore, it is very important to investigate deformation behavior of spherical shell structure under various loads. Updike et al.[2-4] studied the buckling behavior of elastic spherical shell and elastic-plastic spherical shell under quasi-static compression of rigid plate by combining theoretical analysis with experiment, and the theoretical analysis model of hemispherical shell under compression was given and the expressions of displacement and pressure were obtained. Gupta et al.[5-9] investigated the mechanical properties of metal hemispherical shell structures with different radius-thickness ratios subjected to vertical compression. The radius of plastic hinge of metal hemispherical structure was measured by combining experiment, theory and finite element method. The energy dissipation of metal hemispherical structure was studied by using plastic hinge. And a more accurate finite element model was obtained by using experimental data and the effect of different process parameters on the deformation behavior of shell was analyzed. Pauchard et al.[10] studied the failure modes of elastic thin-shell

 doi:10.20944/preprints202208.0063.v1

structures in different situations: contact with a rigid plane and subject to a localized load. The experimental study shows that the failure mode of the sphere in contact with the rigid plate is the flat contact between the shell and the rigid plane; and the second by an inversion of curvature leading to contact with the plane along a circular ridge. Oliveira et al.[11] investigated the failure behavior of rotationally symmetric plastic thin shells under large deflection. The failure modes of conical shell and spherical shell under point load, spherical shell under rigid plate and convex platform load and spherical cap under external uniform pressure are mainly analyzed, and a simple closed solution is obtained for these cases. Amiri et al.[12] studied the semi-spherical elastic-plastic thin shell under concentrated loads at the pole, discussed the relationship between the initial ultimate load and the radius of the bar, and suggested that the ultimate stresses and depression sizes corresponding to large sizes of compression bars are also larger.

All the above studies are for the buckling analysis of continuous spherical shell structures under vertical compression loads. Nevertheless, the mechanical properties of the spherical weave structure proposed in the literature[1] under vertical compression loads have not been studied. In this paper, we combine 3D printing, experiments, and the finite element method (FEM) to analyze the buckling behavior of different types spherical weave structures under vertical compression loads. Compared with other spherical weave structures, the spherical weave with ribbons with in-plane curvatures(new spherical weave structure) not only has a smoother and more continuous geometric configuration, but a higher vertical axial buckling load and initial stiffness, and the new spherical weave structure is more stable. The rest of the paper is organized as follows.

Firstly, the spherical weave structures fabricated by different types of ribbons are analyzed and studied, and it was found that the new spherical weave structure has higher vertical buckling load and initial stiffness, and its structural stability is better. We then study the effect of different ribbon thicknesses and ribbon widths on the vertical buckling load of the new spherical weave structure. Finally, the buckling load expression of the new spherical weave structure under vertical load is proposed, and the finite element analysis is used to obtain the buckling correction coefficient formula related to the ribbon thickness.

II. BUCKLING ANALYSIS OF DIFFERENT SPHERICAL WEAVE STRUCTURES

A. Fabrication of different types of spherical weave structures

We experimentally study the buckling behavior of spherical weave structures under vertical compression load. It can be seen[1] that the spherical weave structure consist of 12 pentagonal and 20 hexagonal unit cells, and the total number of ribbons is 10, each ribbon is evenly divided into 18 segments by rivet hole. According to literature[1], we designed the two spherical weaves: one with straight ribbons, and the other with curved ribbons. The total number of segments of the straight ribbon is 18, and the segment length $l_i^{\circ} = 20mm$; For curved ribbons, the number of segments is 18 and segment curvature $k_i^* = 0.014mm^{-1}$, the segment length $l_i^* = 20mm$. Through the analysis of the above two spherical weave structures, it is found that overall Gaussian curvature of the spherical weave structure $K > 0$, which requires that the Gaussian curvature of the pentagon structure of spherical surface is greater than zero, and that of the hexagon structure is greater than or equal to zero. The formula[1] for calculating the Gaussian curvature of a woven structure is shown below:

$$K_n = \begin{cases} \frac{\pi}{3}(6-n), & \text{With straight ribbons;} \\ \frac{\pi}{3}[6-n(1+\kappa^*)], & \text{With curved ribbons.} \end{cases} \tag{1}$$

Where $\kappa^* = \frac{3}{4\pi}(-\kappa_1 + 2\kappa_2 - \kappa_3)$, $\kappa_i = k_i^* l_i^*$, k_i^* is the segment in-plane curvature of curved ribbon, l_i^* is arc length of curved ribbon. κ_i is the dimensionless curvature of each segment of the curved ribbons. Then the conditions for forming a spherical weave structure are: $K_5 > 0, K_6 \geq 0$. For the spherical weave structure with straight ribbons, the Gaussian curvatures of pentagon and hexagon are: $K_5 = \frac{\pi}{3}, K_6 = 0$, meet the requirements. For the spherical weave structure with curved ribbons, dimensionless curvature of each segment:$(\kappa_1, \kappa_2, \kappa_3) = (0, 0.28, 0)$ for the pentagons and $(\kappa_1, \kappa_2, \kappa_3) = (0.28, 0, 0)$ for the hexagons. And then $K_5 = 0.35, K_6 = 0.42$, all meet the above requirements.

According to the above study, in this paper, we propose a spherical weave structure made of waved ribbons by based on the design method of straight ribbons. Assume that $\kappa^* = 0$, then $\kappa_2 = \frac{\kappa_1+\kappa_3}{2}$. So we take the length and in-plane curvature of segment of waved ribbon is $l_i^w = 20mm$ and $k_i^w = 0.033mm^{-1}$ respectively, so that $\kappa_1 = \kappa_2 = \kappa_3 = 0.66$. Since $\kappa^* = 0$, we can conclude that $K_5 = \frac{\pi}{3}, K_6 = 0$, satisfying the above requirement. The parameters of straight ribbon, ribbon with in-plane curvature, and waved ribbon are shown in Fig. 2.

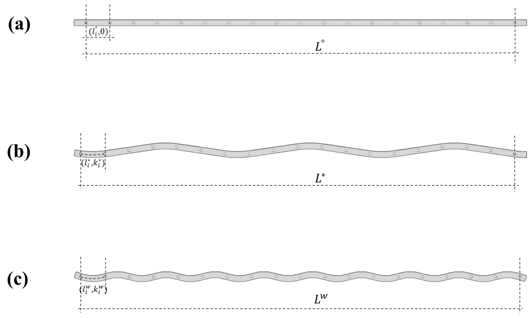

FIG. 1: Different types of ribbons. (a) Straight ribbon, where l_i° is the length of the i-th segment; (b) Ribbon with in-plane curvature, where l_i^* is the arc length of the i-th segment, k_i^* is in-plane curvature of i-th segment; (c) Waved ribbon; where l_i^w is the arc length of the i-th segment of waved ribbon, k_i^w is in-plane curvature of i-th segment of waved ribbon.

To accurately obtain these three kinds of spherical weave structures, we use 3D printing to obtain a single ribbon connected by rivets, using a ZRapid Tech SLA880 3D printer and plastic rivet model is R2024, R2056, R2064. The ribbon material has a elastic modulus of $2000Mpa$, a density of $1.12g/cm^3$, and Poisson's ratio of 0.3. The specific ribbon and plastic rivet details are shown in Figure 2.

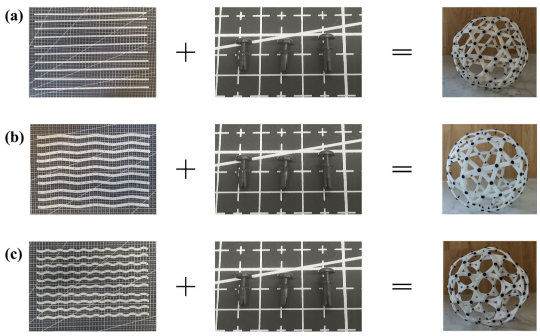

FIG. 2: Different types of spherical weave structures. (a) Spherical weaves with straight ribbons; (b) Spherical weaves with curved ribbons; (c) Spherical weaves with waved ribbons.

By making and observing the spherical weave structure, it is found that the individual ribbons are connected at the beginning and end to form closed circles when woven into the spherical structure, and the center of each ring coincides with the center of the spherical weave structure. Therefore,the total length L of the ribbon is equal to the circumference of the spherical large circle (the center of the circle coincides with the center of the sphere) in the spherical weave structure. In order to obtain the radius of the spherical weave structure, firstly, we derived the equation for the total length of a single ribbon for different types of spherical weave structures respectively. For the spherical weave structure made of straight ribbons, the length of single ribbon is:

$$L^{\circ} = \sum_{i=1}^{n^{\circ}} l_i^{\circ}, \tag{2}$$

Where $n^{\circ} = 18$, l_i° is the length of the i-th segment in the straight ribbons. For the spherical weave structure with curved ribbons, the length of single ribbon is:

$$L^* = \sum_{i=1}^{n^{*1}} \frac{2}{k_i^*} \sin \frac{l_i^* k_i^*}{2} + \sum_{i=1}^{n^{*2}} \cos \frac{l_i^* k_i^*}{2} l_i^*. \tag{3}$$

Where n^{*1} is the number of curved segments in a individual ribbon, n^{*2} is the number of non-curved segments in a individual ribbon, and $n^{*1} + n^{*2} = 18$. For the spherical weave structure with waved ribbons, the length of single ribbon is:

$$L^w = \sum_{i=1}^{n^w} \frac{2}{k_i^w} \sin \frac{l_i^w k_i^w}{2}. \tag{4}$$

Where $n^w = 18$. Then the radii of the different types of spherical weave structures are:

$$R = \begin{cases} \frac{1}{2\pi} \sum_{i=1}^{n^{\circ}} l_i^{\circ}, & \text{With straight ribbons;} \\ \frac{1}{2\pi} (\sum_{i=1}^{n^{*1}} \frac{2}{k_i^*} \sin \frac{l_i^* k_i^*}{2} + \sum_{i=1}^{n^{*2}} \cos \frac{l_i^* k_i^*}{2} l_i^*), & \text{With curved ribbons;} \\ \frac{1}{2\pi} \sum_{i=1}^{n^w} \frac{2}{k_i^w} \sin \frac{l_i^w k_i^w}{2}, & \text{With waved ribbons.} \end{cases} \tag{5}$$

Where $n^{\circ} = 18, n^w = 18, n^{*1} + n^{*2} = 18$, $l_i^{\circ}, k_i^*, l_i^*, k_i^w, l_i^w$ etc. as shown in Figure 1. By the formula(5), the radii of the spherical weave structure fabricated by straight, curved waved ribbon are calculated as follows : $57.3mm$, $56.85mm$ and $56.2mm$, respectively. The actual measured radii of the spherical weave structure are: $57mm$,57.17mm,$57.48mm$. And there is little difference between theory and practice.

B. Experimental Analysis of Different Spherical Weave Structures

In this test, quasi-static vertical compression tests were conducted on a spherical structure woven by straight ribbons (conventional spherical weave structure), a spherical structure woven by ribbons with curved ribbon (new spherical weave structure) and a spherical structure woven by waved ribbons (waved spherical weave structure). The test setup is shown in Figure 3.

Preprints (www.preprints.org) | NOT PEER-REVIEWED | Posted: 2 August 2022 doi:10.20944/preprints202208.0063.v1

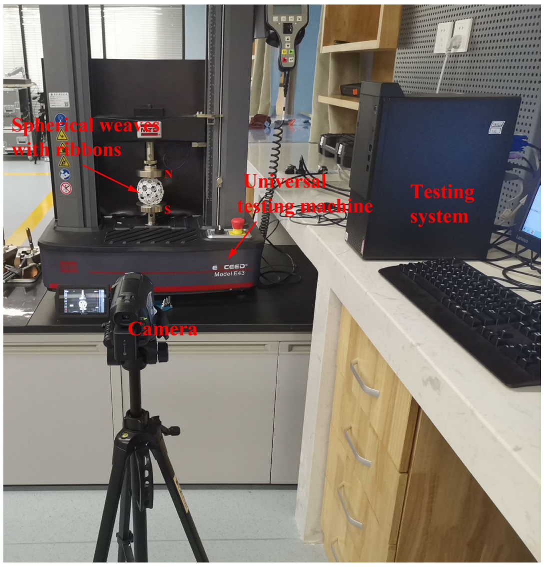

FIG. 3: Testing platform

Displacement control was used in the whole loading process of this test. Before the beginning of the test, the upper pressure head was adjusted to contact the specimen. To ensure the specimen could withstand a quasi-static axial pressure load, the downward pressure velocity of the upper pressure head was $2mm/min$. The load-displacement curves of different spherical weave structures are shown in Fig.4(a), from which it can be seen that the curves of the three spherical weave structures show a trend of increasing and then decreasing. Different degrees of buckling appear in spherical weave structures. Comparing the three different types of spherical weave structures it can be seen that the buckling load of the traditional spherical weave structure is 86% of the new spherical weave structure, and 83% of the waved spherical weave structure; And the buckling load of the new spherical weave structure is not much different from that of the waved spherical weave structure. It is shown that the spherical woven structure with ribbon with curved curvatures has a higher buckling load capacity and its initial stiffness is greater than with straight ribbons and waved ribbons. This is because the spherical weave structure fabricated by naturally curved ribbons has hexagonal Gaussian curvature $K_6 = 0.42$, the spherical Gaussian curvature is more continuous and the structure has a relatively continuous geometric configuration, and the spherical weave structure has good stiffness and stability.

According to the deformation diagrams of different woven structures in Fig. 4(b2-d2), it can be seen that the failure mode of the spherical weave structure under vertical loading can be divided into two stages: a flat contact region forms between the spherical woven structure and the plate, and inward dimple of ribbons. When the spherical weave structure changes from flat contact to inward dimple, the vertical load-displacement curve of the spherical weave structure jumps suddenly, that is, the buckling of the spherical weave structure occurs. In the early stage of loading, flat contact occurs at both the upper and lower poles of the spherical weave structure in contact with the rigid plate; With the increase of the load, the single ribbon of conventional spherical weave structure has a depression at the flat contact part of the north and south poles of the sphere and the rigid plate, and with the increase of vertical displacement, the number of depressed ribbons of the spherical weave structure has increased, and the structure undergoes more serious buckling damage. Compared with the spherical weave structure fabricated by straight ribbon, ribbons with spherical weave structure fabricated using in-plane curvatures ribbons (new spherical weave structures and waved spherical weave structures) are only depressed at one of the north and south poles of the sphere, and as the displacement load increases, the depression deformation continues to increase, and the opposite pole remains flattened. It is indicated that the in-plane curvature of ribbon change the symmetric buckling failure mode of the spherical weave structure, which makes the buckling failure of the structure concentrate on one part of the north and south poles of the spherical structure, and improves the stability of the spherical weave structure.

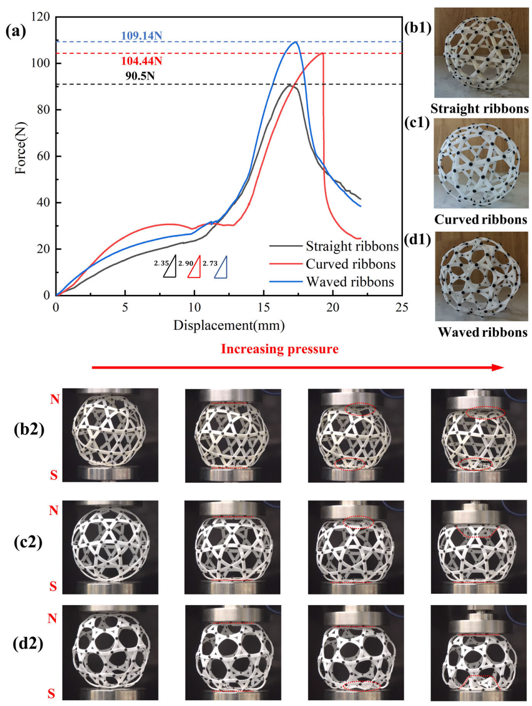

FIG. 4: Test curves and failure modes of different spherical weave structures.

Preprints (www.preprints.org) | NOT PEER-REVIEWED | Posted: 2 August 2022 doi:10.20944/preprints202208.0063.v1

III. THE BUCKLING ANALYSIS OF NEW SPHERICAL WEAVE STRUCTURES

Through the above analysis, it is found that the spherical structure with ribbon with curved curvatures not only has more continuous geometry, but also has good stiffness and stability. To investigate the effect of the width and thickness of ribbons on the new spherical weave structures, we conducted experimental studies on the buckling behavior of spherical weave structures fabricated by naturally curved ribbons. In this paper, six new spherical weave structures with different ribbon thicknesses and ribbon widths are designed and investigated by experimental method. The downward pressure velocity of the upper pressure head was $2mm/min$ and the maximum vertical displacement is $40mm$. The specific parameters of the new spherical weave structure are shown in Table 1.

A. Effect of different thickness of ribbons on new spherical weave structures

To study the influence of the thickness of ribbons in the new spherical weave structures on its buckling mechanical properties, three new spherical weave structures were designed according to different ribbon thicknesses ($h = 0.8, 1, 1.2$). The fabrication process of the specimen ribbon was the same as described above. A diagram of the failure model and the axial load-displacement curve obtained from the test is shown in Fig. 5.

It can be seen from the figure that the new spherical weave structure undergoes two large decreases in the vertical load carrying capacity of the structure when subjected to large vertical displacements, which indicates that the new spherical weave structure buckling twice under vertical loads. Comparing the buckling load values of the three specimens when two buckling occurs, it can be seen that with the increase of ribbon thickness, the vertical load carrying capacity of the new spherical weave structure gradually increases, and the initial stiffness of the structure also gradually increases with the increase of ribbon thickness.

Fig. 5(c-e) is the failure mode diagram of new spherical weave structures with different thickness of curved ribbons. At the early stage of loading, the north and south poles of the new spherical weave structure appeared local flattening, with the increase of displacement load, the ribbons at the south pole of the new spherical weave structure flattened slightly, while the north pole remained flattened. As the displacement load continues to increase, the number of ribbons with concave deforma-

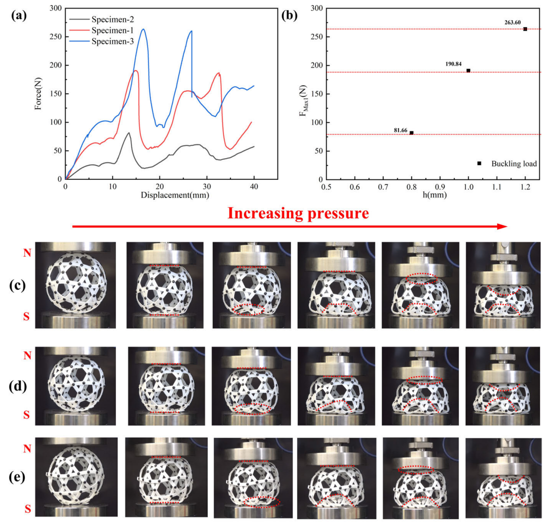

FIG. 5: Test curves and failure modes of new spherical weave structures with different thickness of curved ribbons. (a) Load-displacement curves of new spherical weave structures with different ribbon thicknesses; (b) Scatter plot of the load value F_{Max1} versus ribbon thickness h at the time of first buckling of the structure; (c) The failure modes of Specimen-2; (d) The failure modes of Specimen-1;(e) The failure modes of Specimen-3.

tion at the north pole of the sphere increases, the degree of concavity in the sphere becomes serious, the vertical load carrying capacity of the structure decreases significantly, and the first buckling of the structure occurs. In the middle of loading, the inward dimple of the south pole of the sphere remains unchanged, and the new spherical woven structure has an overall outward rise, the vertical bearing capacity of the structure increases. And then, the single ribbons at the flat contact region of Sphere north pole has inward dimple. At the late stage of loading, a large degree of concavity occurs at the north pole of the new spherical weave structure, at which time a sudden drop in the structural load carrying capacity occurs and the structure undergoes a second buckling. In particular, after the first buckling of Specimen-3, the fracture failure of the ribbon occurred pinned connections in the inward dimple region of the lower part of the structure, and the vertical bearing capacity decreased precipitously. Continuing loading, the inward dimple of ribbons occurs at the north pole of the sphere structure, and the structure undergoes buckling damage. It can be seen that although increasing the ribbon thickness can increase the vertical buckling bearing capacity and initial stiffness of the new spherical weave structure, and improve the stability of the spherical weave structure. The toughness of the spherical weave structure fabricated by thicker ribbons is reduced, and the fracture failure of the ribbon will occur

Preprints (www.preprints.org) | NOT PEER-REVIEWED | Posted: 2 August 2022 doi:10.20944/preprints202208.0063.v1

TABLE I: The parameter of Spherical weaves with curved ribbons

Geometric parameter	Radius	Length	Curvature	Thickness	Width
Unit	$R(mm)$	$l_i^*(mm)$	$k_i^*(mm^{-1})$	$h(mm)$	$b(mm)$
Specimen-1	42.82	15	0.0167	1	5
Specimen-2	42.24	15	0.0167	0.8	5
Specimen-3	42.33	15	0.0167	1.2	5
Specimen-4	42.11	15	0.0167	1	6
Specimen-5	42.38	15	0.0167	1	7
Specimen-6	42.43	15	0.0167	1	8

at the same time as the buckling failure. Fracture failure of new spherical woven ribbons is shown in Figure 6.

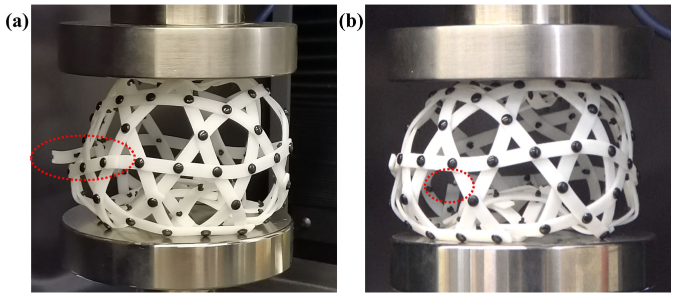

FIG. 6: Fracture failure modes of Specimen-3

B. Effect of different width of ribbons on new spherical weave structures

To explore the influence of different width of ribbons on the compression load of a spherical weave structure composed of naturally curved ribbons, spherical weave structures of ribbons width $b = 5, 6, 7, 8$ were experimentally studied. The other geometric properties of ribbon are shown in Table. 1. The test device of the specimen is shown in Fig. 3. The test loading was controlled by displacement, and the loading rate was $2mm/min$, and the maximum vertical displacement is $40mm$. The load-displacement curve and failure modes obtained from the test is shown in Figure 7

It can be seen from Fig. 7 that when the width of ribbons is $8mm$, the new spherical weave structures has a high initial stiffness and vertical compression buckling load, and its maximum compression buckling load is about twice that of the spherical weave structure with $b = 5mm$ ribbons. With the increase of ribbon width, the buckling load and initial stiffness of the spherical weave structure increase gradually. Analysis of the damage mode diagrams of the four specimens shows that Specimen-1, Specimen-4, Specimen-5, and Specimen-6 all show damage phenomena such as local flattening of

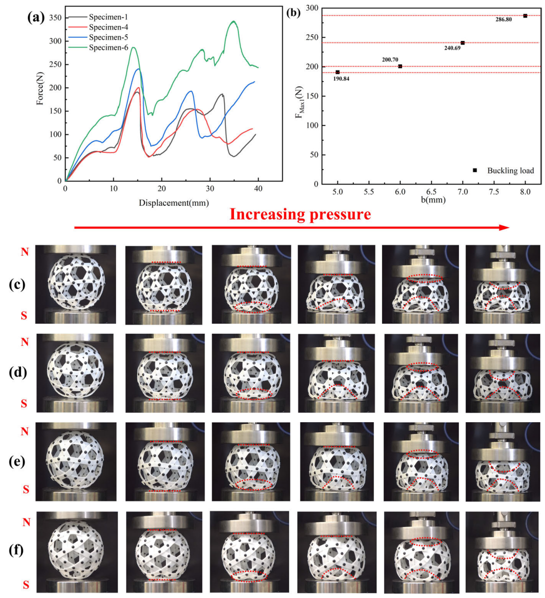

FIG. 7: Test curves and failure modes of new spherical weave structures with different width of curved ribbons.(a) Load-displacement curves of new spherical weave structures with different ribbon widthes;(b) Scatter plot of the load value F_{Max1} versus ribbon thickness h at the time of first buckling of the structure;(c) The failure modes of Specimen-1;(d) The failure modes of Specimen-4;(e) The failure modes of Specimen-5;(f)The failure modes of Specimen-6.

the north and south poles of the spherical structure, internal concave deformation of the ribbon at the sphere flattening, and structural buckling. And all new spherical weave structures appear twice buckling, the structure did not occur fracture failure.

Through the above analysis, it can be concluded that the width of ribbons with in-plane curvatures has a great influence on the buckling bearing capacity of the new spherical weave structures, and increasing the ribbon width can increase the vertical buckling bearing capacity and initial stiffness of the new spherical weave structure, and the structure has better stability.

 doi:10.20944/preprints202208.0063.v1

IV. BUCKLING LOAD OF A NEW SPHERICAL WEAVE STRUCTURE

A. Buckling formula of the new spherical weave structure

From the above test, it can be seen that the new spherical weave structure has better stability. In this section, based on the above tests, combined with the buckling analysis and dimensional analysis of the ribbon, the buckling formula of the new spherical weave structure is given as follows :

$$F_{cr} = n\frac{\pi E}{1-\nu^2}\frac{bh^3}{R^2}. \tag{6}$$

Where n is the number of ribbons, E is the elastic modulus, ν is the Poisson's ratio, b, h is the width and thickness of the ribbons respectively, R is the radius of the spherical weave structure. In order to construct the relationship between the length and in-plane curvature of a single ribbons segment and the buckling load of the spherical weave structure, combined with equation (3), the buckling equation of the new spherical weave structure can be written as:

$$F_{cr} = n\frac{4\pi^3 E}{1-\nu^2}\frac{bh^3}{(\sum_{i=1}^{n^{*1}}\frac{2}{k_i^*}\sin\frac{l_i^* k_i^*}{2} + \sum_{i=1}^{n^{*2}}\cos\frac{l_i^* k_i^*}{2} l_i^*)^2}. \tag{7}$$

Where n^{*1} is the number of curved segments in a individual ribbon, n^{*2} is the number of non-curved segments in a individual ribbon, l_i^* is the arc length of the i-th segment, k_i^* is in-plane curvature of i-th segment; We calculated the vertical buckling load (first buckling) of specimen Specimen-1∼Specimen-6 respectively, and compared the obtained buckling load values of the new spherical weave structure with the test values to verify the accuracy of Equation (7), and the buckling loads of the specific new spherical weave structure are shown in Table 2.

As can be seen from Table 2, there is little difference between the experimental and theoretical values of Specimen-1 vertical buckling load, equation (7) can better predict the buckling load of the new spherical woven structure under vertical load when the ribbon width $b = 5mm$, ribbon thickness $h = 1mm$, and sphere radius $R = 42.82mm$. When the width and thickness of the ribbon are changed, the errors between the experimental and theoretical values of the new spherical weave structure are $0.86 \sim 0.93$, $0.79 \sim 1.01$ respectively. To address this, we propose a buckling correction factor α to correct the theoretical equation of the spherical weave structure, it can be seen from Table 2 that the buckling correction factor is closely related to the thickness and width of a single ribbon. Then the buckling load equation for a spherical woven structure subjected to vertical loads is:

$$F_{cr} \sim \alpha\frac{n\pi E}{1-\nu^2}\frac{bh^3}{R^2}, \tag{8}$$

B. Analysis of Buckling Correction Coefficient

From the above analysis, it can be seen that both ribbon thickness and ribbon width have an effect on the buckling correction factor α of the new spherical weave structure. In contrast, changing the ribbon thickness has a greater effect on the buckling coefficient of the spherical weave structure and there is no pattern. Therefore, we mainly study the influence of different ribbon thickness on the buckling correction coefficient. In this section, the finite element program ABAQUS was used to establish an accurate finite element model of the spherical weave structure in combination with the above tests, to analysis the buckling mechanical properties of new spherical weave structures with different ribbon thicknesses under vertical load. The buckling load values of the new spherical weave structure at different ribbon thicknesses are obtained to determine its buckling correction factor α.

1. Verification of finite element model

Since the ribbons in the spherical weave are connected at the end to form a closed circle, the force-displacement driven modeling method is no longer applicable. In order to obtain the finite element model of the new spherical weave structure accurately and conveniently, the 3D scanner AXE-B17 is used to scan the spherical weave structure in Fig. 2(b), and the scanned model is inverse processed to obtain the finite element model of the spherical weave structure that can be used for calculation. To fully restore the test, we establish a rigid plate in the finite element simulation to simulate the upper pressure head and bottom support of the universal testing machine, respectively. And the upper rigid plate applies vertical displacement; constrains all degrees of freedom of the bottom rigid plate used to simulate the fixed constraints of the bottom support. To simulate the connection of rivets, the overlapping part of two ribbons is coupled to a reference point. Simulation of weaving structure forming using quasi-static in dynamic implicit analysis step. The displacement load is applied, and the loading rate is controlled at $2mm/min$. To speed up the calculation and eliminate the self-locking of mesh shearing, the shell element S4R is used, and the mesh size of

doi:10.20944/preprints202208.0063.v1

TABLE II: Buckling load of a new spherical weave structure

Name	$R(mm)$	b(mm)	h(mm)	$F_{Max1}(N)$	$F_{cr}(N)$	F_{Max1}/F_{cr}
Specimen-1	42.82	5	1	190.84	188.46	1.01
Specimen-2	42.24	5	0.8	81.66	99.07	0.82
Specimen-3	42.33	5	1.2	263.60	332.93	0.79
Specimen-4	42.11	6	1	200.70	233.62	0.86
Specimen-5	42.38	7	1	240.69	269.10	0.89
Specimen-6	42.43	8	1	286.80	306.82	0.93

woven structure is $1mm$. The finite element model uses a material with a modulus of elasticity of $2000Mpa$, a density of $1.12g/cm^3$ and a Poisson's ratio of 0.3. The finite element model and mesh distribution are shown in Fig. 8.

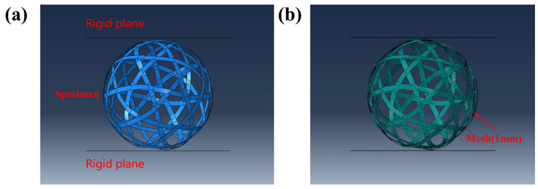

FIG. 8: Finite element model and mesh distribution. The mesh size of rigid plate is $7.5mm$. The mesh size of woven structure is $1mm$.

The above method is used to model the new spherical weave structure by ABAQUS, and the finite element simulation of the new spherical weave structure with different ribbon thicknesses is carried out. To confirm the above modeling method and the finite element model, the new spherical woven structure with thickness $h = 1mm$, width $b = 5mm$ and radius $R = 57.17mm$ is used for simulation, whose results are compared with the test results, as shown in Fig. 9. From Fig. 9(a), we can see that

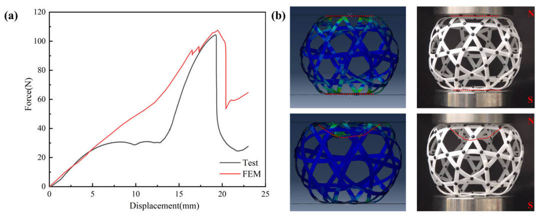

FIG. 9: Verification of finite element model of new spherical weave structure. (a) Comparison of load-displacement curves; (b) Comparison of failure modes.

the initial stiffness of the finite element simulation results is in good agreement with the test, but the maximum buckling load from the simulation is slightly higher than that of the test. Because the coupling approach is used in the finite element simulation to simulate the plastic rivet, but in practice there is a certain gap between the rivet and the rivet hole, which is weaker than the constraint strength of the coupling effect in the finite element. In addition, there are some inevitable errors and initial defects in the test, leads to a slightly higher compression load in the finite element simulation than the test value. In addition, there is a displacement plateau in the test curve, which is due to the fact that realistic spherical weave structures are connected by plastic rivets, and there are certain gaps between ribbons and ribbons and rivets and ribbons. Under vertical load, the outermost rivet end of the structure contacts with the punch head and has a certain angle. With the increase of vertical displacement, the rivet slides with the upper pressure head, and the position of the rigid plate is vertical, and the gap between the ribbons increases; Further loading, the gap between plastic rivet and ribbon, ribbon and ribbon is compacted, which leads to a displacement platform in the load-displacement curve. Since the plastic rivet was not modeled in the simulation, the above displacement plateau did not appear in the finite element simulation.

From the failure mode diagram of the test, it can be seen that the finite element can simulate the flat contact region forms between the spherical weave structure and the plate, and inward dimple of ribbons of the new spherical weave structure in the test, and the overall failure mode of the structure is similar to that of the test, both with multiple ribbons of internal concave buckling at the north pole of the sphere. Compared with the test, it is found that this method can more accurately simulate the vertical compressed mechanical properties of new spherical weave structure in practice.

2. *Finite element parameter analysis*

In order to investigate the effect of ribbon thickness on the buckling correction coefficient of the new spherical weave structure and to ensure that the new spherical weave structure is a thin-shell sphere structure. In this paper, finite element simulations are performed for a new spherical weave structure with ribbon thicknesses ranging from $0.01mm \sim 2.5mm$. The other parameters of the finite element model are consistent with the above. The finite element curves and failure modes of the new spherical weave structures with different ribbon thicknesses are shown in Fig. 10.

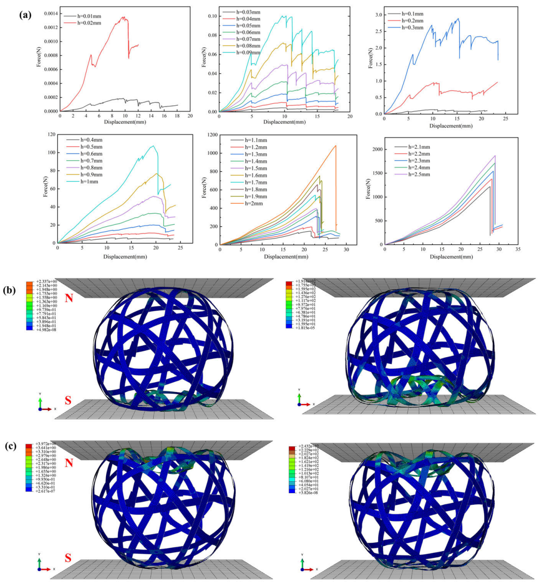

FIG. 10: Finite element curves and failure modes of new spherical weave structures with different thickness of curved ribbons.(a) Load-displacement curves of new spherical weave structures with different ribbon thickness of $0.01mm\ sim 2.5mm$.(b-c)The failure modes for the finite element model of new spherical weave structure.

From Fig. 10(a), we can see that changing the thickness of the curved ribbon, the vertical load carrying capacity of the new spherical weave structure for the first buckling changes significantly. With the increase of ribbon thickness, the buckling load of the new spherical weave structure increases. The models in the finite elements all showed two damage patterns of flat contact region forms between the spherical woven structure and the plate, and inward dimple. The final failure mode of the structure is the concave buckling at the north or south pole of the sphere. The detailed failure modes are shown in Figure 10 (b-c).

In order to facilitate the observation of the relationship between the buckling correction coefficient α and the ribbon thickness, this paper dimensionlessizes the ribbon thickness and investigates the relationship between the dimensionless parameter h/R and the buckling correction coefficient α, where $\alpha = F_{FEM}/F_{cr}$. From Fig. 11(a), when the range of the dimensionless parameter h/R is $0.005 \sim 0.02$, the calculated value of the theoretical formula of the new spherical weave structure is too large, and the buckling load of the actual structure is lower than the theoretical calculation, then equation (7) is not applicable to estimate the buckling load value of the new spherical weave structure under the vertical load. In order to solve this problem, this paper uses a Hook function to fit $\alpha - \frac{h}{R}$ to obtain a lower bound formula for the buckling coefficient of the new spherical weave structure.

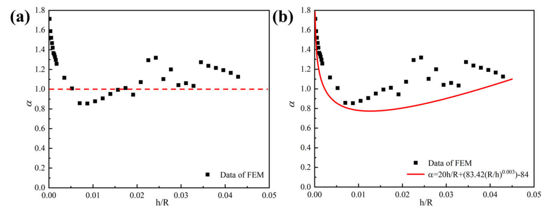

FIG. 11: Buckling loads and buckling correction factorsα for spherically woven structures with different ribbon widths. Where $\alpha = F_{FEM}/F_{cr}$, F_{FEM} is buckling load (first buckling) for the new spherical weave structure using FEM.

From Fig. 11(b), it can be seen that the lower bound fitting equation for the buckling correction factor is:

$$\alpha = 20(\frac{h}{R}) + (83.42(\frac{R}{h})^{0.003}) - 84. \tag{9}$$

Then the buckling load equation for the new spherical weave structure subjected to vertical load is:

$$F_{cr} \sim \alpha n \frac{4\pi^3 E}{1-\nu^2} \frac{bh^3}{\left(\sum_{i=1}^{n^{*1}} \frac{2}{k_i^*} \sin\frac{l_i^* k_i^*}{2} + \sum_{i=1}^{n^{*2}} \cos\frac{l_i^* k_i^*}{2} l_i^*\right)^2}. \tag{10}$$

To validate formula (10), we calculate the buckling load of Specimen-2 and Specimen-3, and compare the obtained buckling load value with the experimental data. The specific results are shown in Table 3.

From Table 3, we can see that the buckling load of the new spherical weave structure calculated by formula (10) is not much different from the experimental buckling load. The error of the results of the two models is 1.03 and 0.90, respectively. This shows that using the buckling correction factor α to correct Formula (6) can better reflect the buckling load of the new spherical weave structure under vertical load.

V. CONCLUSION

We studied the buckling behavior of different spherical weave structure under vertical loads by combining experimental and finite element methods. It was demonstrated that, the deformation of the spherical weave structure under the vertical compressive load can be divided into 2 stages: a flat contact region forms between the spherical weave structure and the rigid plate and inward dimple. Conventional spherical weave structures are subjected to vertical loads, with simultaneous buckling of

TABLE III: Comparisons of test results with those from Eqs. (10)

Name	$R(mm)$	$h(mm)$	$b(mm)$	h/R	$F_{Max1}(N)$	$F_{cr}(N)$	error
Specimen-2	42.24	0.8	5	0.0189	81.66	78.97	1.03
Specimen-3	42.33	1.2	5	0.0283	263.6	294.14	0.90

the north and south poles of the sphere at the contact locations with the rigid plate. However, the new woven structure first buckles on the south or north pole side of the sphere, and the corresponding buckling occurs on the other side of the sphere with the increase of load. Compared with the traditional spherical weave structure and waved spherical weave structure, the new woven spherical structure with naturally curved (in-plane) ribbons has higher initial stiffness and a larger buckling load. In addition, we investigated the effect of different thickness h and width b of ribbons on the buckling behavior of the new woven spherical structure. Experimental studies show that increasing the thickness and width of the ribbon can increase the vertical buckling bearing capacity and initial stiffness of the new woven spherical structure, and improve the stability of the spherical weave structure. But excessively thick ribbons can lead to fracture failure of ribbon of the new woven spherical structure. Finally, the buckling load equation and buckling correction coefficient of the new spherical weave structure under vertical load are proposed in this paper by combining buckling analysis and dimensional analysis of the ribbon structure, and the buckling correction coefficient equation related to the ribbon thickness is obtained by finite element calculation.

[1] Baek C, Martin A G, Poincloux S, et al. Smooth triaxial weaving with naturally curved ribbons. Physical Review Letters, 2021, 127(10): 104301.

[2] Updike, Dean Pierson, and Arturs Kalnins. Axisymmetric behavior of an elastic spherical shell compressed between rigid plates. 1970, 635-640.

[3] Updike, Dean Pierson, and Arturs Kalnins. Axisymmetric postbuckling and nonsymmetric buckling of a spherical shell compressed between rigid plates. 1972: 172-178.

[4] Updike, Dean Pierson. On the large deformation of a rigid-plastic spherical shell compressed by a rigid plate. 1972: 949-955.

[5] Gupta N K, Sheriff N M, Velmurugan R. Experimental and theoretical studies on buckling of thin spherical shells under axial loads. International journal of mechanical sciences, 2008, 50(3): 422-432.

[6] Gupta N K, Prasad G L E, Gupta S K. Axial compression of metallic spherical shells between rigid plates. Thin-walled structures, 1999, 34(1): 21-41.

[7] Gupta N K. Experimental and numerical studies of dynamic axial compression of thin walled spherical shells[J]. International journal of impact engineering, 2004, 30(8-9): 1225-1240.

[8] Gupta N K, Sheriff N M, Velmurugan R. Experimental and numerical investigations into collapse behaviour of thin spherical shells under drop hammer impact. International journal of solids and structures, 2007, 44(10): 3136-3155.

[9] Gupta P K, Gupta N K. A study of axial compression of metallic hemispherical domes. Journal of materials processing technology, 2009, 209(4): 2175-2179.

[10] Pauchard L, Rica S. Contact and compression of elastic spherical shells: the physics of a ping-pongball. Philosophical Magazine B, 1998, 78(2): 225-233.

[11] De Oliveira J G, Wierzbicki T. Crushing analysis of rotationally symmetric plastic shells. The Journal of Strain Analysis for Engineering Design, 1982, 17.4: 229-236.

[12] Amiri S N, Rasheed H A. Plastic buckling of moderately thick hemispherical shells subjected to concentrated load on top[J]. International Journal of Engineering Science, 2012, 50(1): 151-165.